# Discretized Modal Shock Response of a Homogeneous, Damped, Rectangular Plate

R. David Hampton
Mechanical Engineering Division
U. S. Military Academy
West Point, NY

Ting H. Li
Ordnance Materials Branch
Weapons & Materials Research Directorate
U. S. Army Research Laboratory
Adelphi, MD

Kip P. Nygren
Civil & Mechanical Engineering Department
U. S. Military Academy
West Point, NY

## 1 Executive Summary

Ballistic shock, the strong vibrations that propagate through a vehicle structure after a ballistic impact, can damage electronic components that are mounted on various interior locations of the vehicle. To protect onboard critical electronic components from ballistic shock damage, predicted shock response spectra (SRS) are used as design guidelines in the selection of shock isolation devices. Current technology to predict shock response intensity at component mounting locations include Finite Element Analysis and Statistical Energy Analysis, along with various other modeling approaches. The Army Research Laboratory is implementing a process to determine component damage probability based on a numerical modal superposition method. This process allows detailed modeling of an entire vehicle (including instrumentation racks) but requires months of effort to perform skillful FEA modeling. Such an expenditure is acceptable only for selected high-value vehicles, and is impractical for analysis of many vehicles. Therefore it is desirable to investigate alternative shock analysis methods that are simple and general (i.e., independent of specific vehicle configurations). Although such methods could entail reduced accuracy, for some situations they would eliminate the need for time-consuming finite element modeling, and could provide analyses useful with a variety of vehicles. As such, the methods could be used for "screening" for rapid identification of potential shock-damage issues. If necessary, further detailed analysis could be accomplished subsequently.

When an armored vehicle is subjected to a non-perforating large-caliber munitions impact or blast, direct-mounted components near the impact location will always risk the

highest damage potential. Live-fire ballistic tests and laboratory experiments as well as numerical modeling have proven this observation. The research presented in this paper develops a constant- and lumped-parameter linear matrix model of a homogeneous, rectangular plate subject to transverse ballistic shock, for two classes of boundary conditions: (1) all edges in simple support, and (2) edges alternating between simple and clamped (fixed) support as one proceeds around the perimeter. Damping is included in Rayleigh and modal forms. The matrix models are provided in a form suitable for eigen-analysis intended to yield kinematic responses for SRS determination. The enabled "same-plate" shock analysis, while not encompassing an entire military vehicle, would treat the most severe cases of shock response, for components mounted directly on the impacted plate.

## 2 Introduction

Military equipment must be designed to operate under a variety of hostile environmental conditions. Mechanical shocks, such as blast loads or projectile impacts on military platforms, often place debilitating demands on critical electronic and other military subsystems. These component failures can in turn disable the military platforms they support even when the impacts themselves are humanly survivable.

Various types of shock response spectra (SRSs) [1, 2] are commonly used as analytical tools for the design and analysis of military hardware that will likely be subject to remote impulsive shock loading. The remote impulse is filtered through the eigenstructure of the military platform to the attachment point of the supporting subsystem, which is in turn excited via its composite modes. A single point on a SRS curve graphically represents the maximum time response of a hypothetical single-degree-of-freedom (SDOF) mass-spring-damping (MSD) system, assumed to be attached in some desired direction at a contemplated or actual subsystem attachment point. A complete SRS comprises a curve of the selected maximum response (typically absolute acceleration, relative position, or pseudovelocity [3, 4]) plotted as a function of SDOF-system frequency, for a single damping ratio. Figure 1 represents a shock-loaded system *S* with remote impact at point *C* and SDOF system attached at point *D*. A single point $(\omega_n, S_V)$ of an undamped pseudovelocity shock response spectrum (PSRS), for example, would represent the maximum relative position $x-d$ of mass *m*, over time, multiplied by undamped natural frequency $\sqrt{k/m}$, plotted versus that frequency:

$$S_V(\omega_n) := \omega_n \left| x(t) - d(t) \right|_{\max}. \tag{1}$$

For definitions of other common types of SRS, refer to [4].

The approach employed by most analysts for determining the respective responses at a set of *r* attachment points, $D_i$, to an input at *C*, is to use direct integration via a finite element analysis model. For each impact point of interest on supported system *S*, the integration process must be repeated. This is a very time-consuming process. For a

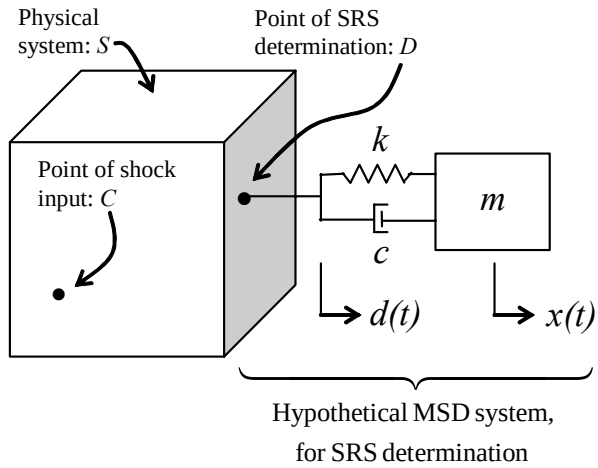


Figure 1. Shock-loaded system *S*,
with (hypothetical) attached MSD system
for SRS determination

typical Stryker-vehicle analysis using, say, 1E5 shell elements and 1500 impact points, this approach takes about two days per impact for a set of attachment points. Although it is too slow for many impacts, the method can be used for comparison in a few cases.

If the region of plastic deformation due to the impact is small, so that modal superposition can be used, the process is significantly faster. For a Stryker vehicle analysis using 1E5 shell elements and 500 modes, the modal analysis time is about 72 hours. The subsequent transient analysis time for a set of attachment points then takes about 10 minutes, for each impact location. Though much faster than the direct integration approach, with 1500 impact points the transient analysis time is still about 10 days. Then the response of the attached SDOF system must be evaluated numerically via a convolution integral (or some approximation of one) for each desired combination of impulse shape, impact location, attachment point, attached-system damping ratio, and attached-system natural frequency. The results from either approach are typically compiled in a huge database for use in subsystem design and analysis. Due to the immense computational overhead required with either of the above processes, methods are being sought which can speed up SRS development for a supported military platform.

As noted above, modal analysis offers the faster of the two routes to attachment-point transient response, provided the system model can be assumed to be linear (as is frequently realistic for point impacts). If the remote shock input (e.g., at *C*, Fig. 1) can be idealized as a Dirac-delta function, then for Rayleigh or modal damping with symmetric mass and stiffness matrices the attachment-point transient response (e.g., at point *D*, Fig. 1) can be determined analytically from the basic platform's modal structure [5, 6]. In these cases, the system response is found using $2^{nd}$-order linear matrix differential equations. For more general damping or with an asymmetric mass or stiffness matrix a $1^{st}$-order linear matrix differential equation (i.e., state-space form) can be used [7]. In any of the above cases the response will be a linear combination of exponentially

decaying sinusoids of known parameters. With Rayleigh damping the response has also been determined analytically for other idealizations of the remote input—such as a rectangular pulse or a sawtooth pulse [6]. The existence of an analytical solution, as in any of the foregoing cases, means that the appropriate structure (modal or eigen-) of the basic platform need be determined only once, irrespective of the number of impacts or attachment points. This in turn offers an enormous savings in modeling and computational time and effort.

Further, from these analytical solutions the SDOF system's kinematic response can also be determined analytically [5, 6, 7]. Consequently, each convolution integral that would otherwise be required to determine an SRS (i.e., for each undamped natural frequency and damping ratio, at each attachment point), can be replaced with an algebraic equation. The computational savings is not significant for any single data point on an individual SRS plot; but since the number of convolutions that must be performed to develop the platform's data base can be several hundred thousand, the additional computational savings can be quite substantial. Additionally, use of algebraic kinematic responses, for attachment point and for SDOF-system mass, means that SRS data points can be determined exactly for arbitrarily low frequencies. This would not be possible if nonalgebraic means were used for evaluating the convolution integrals [3].

The above paragraphs address the computational savings from impact idealization, system linearization, modal- or eigen-decomposition, and a priori (algebraic) convolution. It is also possible, with some platforms, to represent an impacted surface by a plate with idealized geometry, material properties, and boundary conditions. For many such cases exact continuous solutions, or continuous solution-approximations or bounds, exist in the literature [8, 9, 10]. The simplest case for which an exact solution exists is a homogeneous, undamped rectangular plate, simply supported on all edges, and subjected to a transverse external force density. With these boundary conditions the eigenstructure can be represented explicitly. Previously [11] the authors developed and solved algebraically, from this continuous solution, a linear, constant-parameter, lumped-parameter, dynamical model of a homogeneous, simply-supported rectangular plate, to include either Rayleigh or modal damping. The present paper repeats that development, and extends the approach to the more difficult case in which the boundary conditions for the four edges alternate between simply-supported and clamped as one proceeds around the perimeter of the plate.

## 3 General Scenario

Consider a flat, linear, homogenous rectangular plate (Fig. 2) of length $a$ ($x$-direction), width $b$ ($y$-direction), uniform thickness $h$, Young's modulus $E$, Poisson's ratio $\nu$, and mass density $\rho$ per unit area. The plate is simply supported on two opposing edges; on the other two edges the boundary conditions are either both simply supported (Case 1) or both clamped (Case 2). Assume the plate to be subject to a time-varying transverse external force intensity (i.e., per unit area of plate surface):

$$q = q(x, y, t), \tag{2}$$

with the $x$ and $y$ axes lying in the undeformed neutral plane. Finally, the plate is assumed to have either modal or Rayleigh damping.

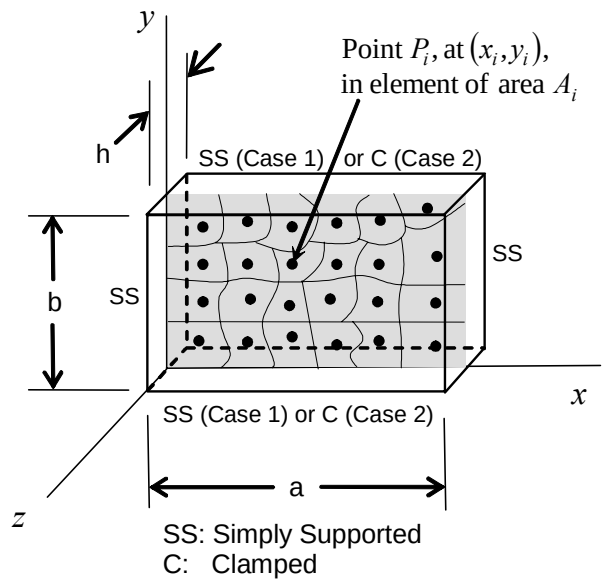


Figure 2. Plate with opposing simple supports, to be discretized

The partial differential equation for the undamped plate is well-known (e.g., [9, p. 257]):

$$\rho w_{tt} + D\nabla^4 w = q(x, y, t); \tag{3}$$

where

$$w = w(x, y, t) \tag{4}$$

is the transverse ($z$-direction) displacement of the neutral surface,

the flexural rigidity $D$ is defined by

$$D = \frac{Eh^3}{12\left(1-\nu^2\right)}, \tag{5}$$

the subscript notation indicates partial differentiation:

$$w_{tt} := \frac{\partial^2 w}{\partial t^2}, \tag{6}$$

and

$$\nabla^4 := \nabla^2 \nabla^2 \tag{7}$$

is the biharmonic differential operator (the dual application of the Laplacian operator $\nabla^2$). For rectangular coordinates the Laplacian is expressed by

$$\nabla^2 = \frac{\partial^2}{\partial x^2} + \frac{\partial^2}{\partial y^2} . \tag{8}$$

The goals of this paper are as follows:

(a) to use the plate's partial differential equation (3) and its undamped solution, given the selected boundary conditions (i.e., either all edges simply supported, or supports alternating between simple and clamped), to develop a lumped-parameter differential equation for the damped plate in a useful linearized matrix form;

(b) to use the matrix differential equation of motion to determine analytically the response of the plate at arbitrary point $(x_j, y_j)$ to an impulsive shock input at a different arbitrary point $(x_i, y_i)$; and

(c) to use the response solution at $(x_j, y_j)$ to determine analytically the kinematic quantities needed for SRS computation at $(x_j, y_j)$, under the assumption of various types of idealized impulsive loading at $(x_i, y_i)$.

# 4 Case One: Simply Supported Edges

## 4.1 Free Response of the Continuous Undamped Plate

Consider first the case where the plate is simply supported on all four edges, and responding freely to initial conditions. The simply supported boundary conditions [9] are represented by

$$w = w_{xx} + \nu w_{yy} = 0 . \tag{9}$$

An analytical, modal solution to the homogeneous form of the undamped differential equation is well known, for this plate geometry and set of boundary conditions. In particular,

$$w(x, y, t) = \sum_{m=1}^{\infty} \sum_{n=1}^{\infty} W_{mn}(x, y) \eta_{mn}(t), \tag{10}$$

where undamped natural frequency *mn* is

$$\omega_{mn} = \sqrt{\frac{D}{\rho}} \pi^2 \left[ \left( \frac{m}{a} \right)^2 + \left( \frac{n}{b} \right)^2 \right], \tag{11}$$

the associated modeshape is

$$W_{mn} = C_{mn} \sin\left(\frac{m\pi x}{a}\right)\sin\left(\frac{n\pi y}{b}\right), \tag{12}$$

and the corresponding undamped modal coordinate is

$$\eta_{mn} = \sin\left(\omega_{mn} t + \phi_{mn}\right). \tag{13}$$

Constants $C_{mn}$ and $\phi_{mn}$ depend on the initial conditions.

If the undamped natural frequencies are arranged in increasing order, then indices *mn* can be replaced with a single index *k*, and (10) through (13) can be rewritten as follows:

$$w(x, y, t) = \sum_{k=1}^{\infty} W_k(x, y)\eta_k(t) \tag{14}$$

where the $k^{th}$ undamped natural frequency is

$$\omega_k = \sqrt{\frac{D}{\rho}}\,\pi^2\left[\left(\frac{m}{a}\right)^2 + \left(\frac{n}{b}\right)^2\right], \tag{15}$$

the associated modeshape is

$$W_k = C_k \sin\left(\frac{m\pi x}{a}\right)\sin\left(\frac{n\pi y}{b}\right) = C_k \sin\left(\frac{m\pi x}{a}\right)\sin\left(y\sqrt{\omega_k\sqrt{\frac{\rho}{D}} - \left(\frac{m\pi}{a}\right)^2}\right), \tag{16}$$

and the corresponding undamped modal coordinate is

$$\eta_k = \sin\left(\omega_k t + \phi_k\right). \tag{17}$$

## 4.2 Forced Response of the Discretized Damped Plate

### 4.2.1 Matrix differential equation of motion

In terms of differential mass elements

$$dm = \rho dA, \tag{18}$$

(3) can be re-expressed, still for the continuous system, as

$$(\rho dA)w_{tt} + (DdA)\nabla^4 w = q(x, y)dA. \tag{19}$$

To express the mathematical model in finite-dimensional form, first discretize the plate into $r$ elements of respective areas $A_i$ $(i = 1,...,r)$, with the mass

$$m_i = \rho A_i \tag{20}$$

of the $i^{th}$ element located in the element on the neutral surface, at some point $P_i$ having coordinates $(x_i, y_i)$. (Refer to Fig. 2.) The fidelity of the discretized representation can be expected to vary, of course, depending on the choices both of the value of $r$ and of the locations of points $P_i$; a reasonable location for $P_i$ would be at the centroid of the $i^{th}$ mass element. Lump the transverse loading on the $i^{th}$ element into concentrated force

$$f_i(t) = \int_{A_i} q(x, y)dA_i, \tag{21}$$

applied at $P_i$. Then for the $i^{th}$ element (19) becomes

$$m_i\, w_{tt}\big|_{(x_i, y_i)} + (DA_i)\nabla^4 w\big|_{(x_i, y_i)} = f_i. \tag{22}$$

In vector form, using transparent notation for the vector elements,

$$\underbrace{\begin{bmatrix} m_1 & & \\ & \ddots & \\ & & m_r \end{bmatrix}}_{M} \underbrace{\begin{Bmatrix} \ddot{w}_1 \\ \\ \ddot{w}_r \end{Bmatrix}}_{\underline{\ddot{w}}} + D \underbrace{\begin{Bmatrix} A_1 \nabla^4 w_1 \\ \vdots \\ A_r \nabla^4 w_r \end{Bmatrix}}_{DA\nabla^4 \underline{w}} = \underbrace{\begin{Bmatrix} f_1 \\ \vdots \\ f_r \end{Bmatrix}}_{\underline{f}}, \tag{23}$$

where

$$A = \begin{bmatrix} A_1 & & \\ & \ddots & \\ & & A_r \end{bmatrix} \tag{24}$$

and

$$M = \rho A. \tag{25}$$

Application of the biharmonic operator to (14) leads directly to

$$\nabla^4 w = \nabla^4 \left[ \sum_{k=1}^{\infty} W_k(x,y)\eta_k(t) \right] = \sum_{k=1}^{\infty} \left\{ \nabla^4 \left[ W_k(x,y) \right] \eta_k(t) \right\}. \tag{26}$$

Expanding $\nabla^4$ in terms of rectangular coordinates via (8), applying it to (26), and approximating the modal sum by the first *r* terms, yields

$$\nabla^4 w = \frac{\rho}{D} \sum_{k=1}^{r} \omega_k^2 W_k(x,y)\eta_k(t). \tag{27}$$

The modeshapes can be discretized into vector form:

$$\underline{u}_k = \begin{Bmatrix} C_k \sin\left(\dfrac{m\pi x_1}{a}\right)\sin\left(\dfrac{n\pi y_1}{b}\right) \\ \vdots \\ C_k \sin\left(\dfrac{m\pi x_r}{a}\right)\sin\left(\dfrac{n\pi y_r}{b}\right) \end{Bmatrix}, \tag{28}$$

which can be normalized using the Euclidean norm:

$$\underline{m}_k = \frac{\underline{u}_k}{\left|\underline{u}_k\right|}. \tag{29}$$

Define $r \times p$ modeshape matrix

$$U = \left[ \underline{m}_1, \ldots, \underline{m}_p \right], \tag{30}$$

and use it to define a normalized modal coordinate vector $\underline{\eta}$ as follows:

$$\underline{w} = U\underline{\eta}. \tag{31}$$

It should be noted here that the number *p* of modes comprising *U* can never exceed half the number *r* of mass elements—and in many cases *p* must be considerably smaller—in order to avoid spatial aliasing effects. In particular, for a rectangular plate comprising *r* equal rectangular elements of dimensions $\Delta x \times \Delta y$, discretized modeshape $\underline{u}_k$ cannot represent continuous modeshape $W_k$ without aliasing unless

$$\Delta x < a / m \tag{32}$$

and

$$\Delta y < b / n \tag{33}$$

for the particular values of $m$ and $n$ corresponding to $W_k$ (and $\underline{u}_k$).

Now, using (31), (25), and (27), the discretized equation of motion (23) can be expressed in terms of modal coordinates by

$$MU\ddot{\underline{\eta}} + MU\Omega^2\underline{\eta} = \underline{f}\,, \tag{34}$$

for

$$\Omega = \begin{bmatrix} \omega_1 & & \\ & \ddots & \\ & & \omega_p \end{bmatrix}. \tag{35}$$

In terms of physical coordinates, and using $U^+$ to represent the pseudoinverse of $U$,

$$M\ddot{\underline{w}} + K\underline{w} = \underline{f}\,, \tag{36}$$

where

$$K = MU\Omega^2U^+\,. \tag{37}$$

The pseudoinverse $U^+$ was required above in lieu of the normal inverse, since $U$ is not square.

It should be noted here, for subsequent use, that although mass matrix $M$ is symmetric—and diagonal (23)—stiffness matrix $K$ is not necessarily even symmetric, as one can show readily by using $r = 2$ and solving for $K$ algebraically. Further, the discretized modeshape matrix $U$ is not necessarily unitary.

One can now insert modal damping into (34). First premultiply each term of (34) by $(MU)^+$ to obtain

$$\ddot{\underline{\eta}} + \Omega^2\underline{\eta} = (MU)^+\underline{f}\,. \tag{38}$$

Define a modal damping matrix by

$$C_M = \begin{bmatrix} 2\varsigma_1\omega_1 & & \\ & \ddots & \\ & & 2\varsigma_p\omega_p \end{bmatrix}. \tag{39}$$

Then from (38) the damped equations are

$$\ddot{\underline{\eta}} + C_M\dot{\underline{\eta}} + \Omega^2\underline{\eta} = (MU)^+\underline{f}\,. \tag{40}$$

Note that these equations are decoupled. In terms of physical coordinates, via (31), (40) reduces to

$$M\underline{\ddot{w}}+C\underline{\dot{w}}+K\underline{w}=\underline{f}\,, \tag{41}$$

where
$$C=MUC_M U^+\,, \tag{42}$$

and $K$ is as defined previously, by (37).

Alternatively, with Rayleigh damping, (36) becomes

$$M\underline{\ddot{w}}+C_R\underline{\dot{w}}+K\underline{w}=\underline{f}\,, \tag{43}$$

where
$$C_R=\alpha M+\beta K\,, \tag{44}$$

for some desired $\alpha$, $\beta$. In terms of modal coordinates, (43) is

$$MU\underline{\ddot{\eta}}+C_R U\underline{\dot{\eta}}+MU\Omega^2\underline{\eta}=\underline{f}\,, \tag{45}$$

or
$$\underline{\ddot{\eta}}+(MU)^+C_R U\underline{\dot{\eta}}+\Omega^2\underline{\eta}=(MU)^+\underline{f}\,. \tag{46}$$

This reduces in turn to the decoupled set of equations

$$\underline{\ddot{\eta}}+\Gamma\,\underline{\dot{\eta}}+\Omega^2\underline{\eta}=(MU)^+\underline{f}\,, \tag{47}$$

where, using $r\times r$ identity matrix $I$,

$$\Gamma=\alpha I+\beta\Omega^2=\begin{bmatrix}\alpha+\beta\omega_1^2 & & \\ & \ddots & \\ & & \alpha+\beta\omega_p^2\end{bmatrix}. \tag{48}$$

Alternatively expressed,

$$\Gamma=\alpha I+\beta\Omega^2=\begin{bmatrix}2\varsigma_1\omega_1 & & \\ & \ddots & \\ & & 2\varsigma_p\omega_p\end{bmatrix}, \tag{49}$$

where
$$\varsigma_i = \frac{\alpha + \beta\,\omega_i^2}{2\omega_i}. \tag{50}$$

Observe that since $K$ is not symmetric, and since $U$ is not unitary, the usual unitary similarity transformation $U^*(\cdot)U$ has not been (cannot be) used to diagonalize the damping or stiffness matrix in either (41) or (43). However, (40) and (47) still represent the respective modal equations in decoupled form.

### 4.2.2 Response $w(x_j, y_j, t)$ to shock input $f(x_i, y_i, t)$

Using Laplace transforms, and assuming all modes to be underdamped, the $i^{th}$ modal solution to either (40) or (47) is

$$\eta_i(t) = e^{-\varsigma_i \omega_{ni} t}\left(A_i \cos\omega_{di} t + B_i \sin\omega_{di} t\right) + \frac{1}{\omega_{di}}\left(e^{-\varsigma_i \omega_{ni} t}\sin\omega_{di} t\right) * \tilde{f}_i\,, \tag{51}$$

where
$$A_i = \eta_i\left(0^+\right), \tag{52}$$

$$B_i = \frac{\varsigma_i \omega_{ni}}{\omega_{di}}\eta_i\left(0^+\right) + \frac{1}{\omega_{di}}\dot{\eta}_i\left(0^+\right), \tag{53}$$

and $\tilde{f}_i$ is the $i^{th}$ element of $(MU)^+ \underline{f}$.

In matrix form, the modal coordinate vector is

$$\underline{\eta}(t) = \begin{bmatrix} e^{-\varsigma_1 \omega_{n1} t}\left[\cos\omega_{d1} t + \left(\frac{\varsigma_1 \omega_{n1}}{\omega_{d1}}\right)\sin\omega_{d1} t\right] & & \\ & \ddots & \\ & & e^{-\varsigma_p \omega_{np} t}\left[\cos\omega_{dp} t + \left(\frac{\varsigma_p \omega_{np}}{\omega_{dp}}\right)\sin\omega_{dp} t\right] \end{bmatrix} \underline{\eta}(0+)$$

$$+ \begin{bmatrix} \left(\frac{1}{\omega_{d1}}\right)e^{-\varsigma_1 \omega_{n1} t}\sin\omega_{d1} t & & \\ & \ddots & \\ & & \left(\frac{1}{\omega_{dp}}\right)e^{-\varsigma_p \omega_{np} t}\sin\omega_{dp} t \end{bmatrix} \dot{\underline{\eta}}(0+)$$

$$+\begin{bmatrix} \left(\frac{1}{\omega_{d1}}\right)e^{-\varsigma_1\omega_{n1}t}\sin\omega_{d1}t & & \\ & \ddots & \\ & & \left(\frac{1}{\omega_{dp}}\right)e^{-\varsigma_p\,\omega_{np}t}\sin\omega_{dp}t \end{bmatrix} * (MU)^+\,\underline{f}(t) \Bigg\}. \qquad (54)$$

Accordingly, upon applying (31), the physical coordinate vector is

$$\underline{w}(t) = U\left\{\begin{bmatrix} e^{-\varsigma_1\omega_{n1}t}\left[\cos\omega_{d1}t + \left(\frac{\varsigma_1\omega_{n1}}{\omega_{d1}}\right)\sin\omega_{d1}t\right] & & \\ & \ddots & \\ & & e^{-\varsigma_p\omega_{np}t}\left[\cos\omega_{dp}t + \left(\frac{\varsigma_p\omega_{np}}{\omega_{dp}}\right)\sin\omega_{dp}t\right] \end{bmatrix} U^+\underline{w}(0+)\right.$$

$$+\begin{bmatrix} \left(\frac{1}{\omega_{d1}}\right)e^{-\varsigma_1\omega_{n1}t}\sin\omega_{d1}t & & \\ & \ddots & \\ & & \left(\frac{1}{\omega_{dp}}\right)e^{-\varsigma_p\,\omega_{np}t}\sin\omega_{dp}t \end{bmatrix} U^+\dot{\underline{w}}(0+)$$

$$\left.+\begin{bmatrix} \left(\frac{1}{\omega_{d1}}\right)e^{-\varsigma_1\omega_{n1}t}\sin\omega_{d1}t & & \\ & \ddots & \\ & & \left(\frac{1}{\omega_{dp}}\right)e^{-\varsigma_p\,\omega_{np}t}\sin\omega_{dp}t \end{bmatrix} * (MU)^+\,\underline{f}(t)\right\}. \qquad (55)$$

Suppose that the only nonzero element of $\underline{f}$ is a shock input

$$f_i = f\left(x_i, y_i, t\right), \qquad (56)$$

applied to point $P_i$. Let the $(i, j)$ elements of $U$ and $U^+$ be represented by $u_{ij}$ and $v_{ij}$. Then for zero initial conditions (55) reduces readily to

$$\underline{w}(t) = \left[\underline{m}_1, \ldots, \underline{m}_p\right]\begin{Bmatrix} \frac{1}{\omega_{d1}}\,e^{-\varsigma_1\omega_{n1}t}\sin\omega_{d1}t * \sum_{i=1}^{r}\frac{v_{1i}}{m_i}f_i(t) \\ \vdots \\ \frac{1}{\omega_{dp}}\,e^{-\varsigma_p\omega_{np}t}\sin\omega_{dp}t * \sum_{i=1}^{r}\frac{v_{pi}}{m_i}f_i(t) \end{Bmatrix}, \qquad (57)$$

from which the displacement response $w_j$ (at point $P_j$) to the force input $f_i$ (at $P_i$) is

$$w_j(t) = \frac{f_i(t)}{m_i} * \sum_{k=1}^{p} \left( \frac{u_{jk} v_{ki}}{\omega_{dk}} \right) e^{-\varsigma_k \omega_{nk} t} \sin \omega_{dk} t \,. \tag{58}$$

If the shock input can be idealized as a Dirac delta of strength $\gamma$, the response is simply the sum of $p$ exponentially decaying sinusoids:

$$w_j(t) = \frac{\gamma}{m_i} \sum_{k=1}^{p} \left( \frac{u_{jk} v_{ki}}{\omega_{dk}} \right) e^{-\varsigma_k \omega_{nk} t} \sin \omega_{dk} t \,, \tag{59}$$

as expected. Adding to (59) the effects of initial conditions, from (55), is straightforward, and not included here.

For certain other deterministic inputs $f_i$ (e.g., rectangular, sawtooth, haversine, or versed-sine impulses) the right-hand side of (58) can also be evaluated as an algebraic expression, upon performing the associated convolution integration analytically (rather than numerically). Reference [6] shows the procedure for ideal-impulse (Dirac-delta), rectangular-pulse, and sawtooth-pulse inputs, in the related case of symmetric mass and stiffness matrices with Rayleigh damping. For the case of more general damping, and with asymmetric mass and/or stiffness matrices (as here), [7] provides a general procedure using a state-space approach; and achieves an algebraic solution for a Dirac-delta shock input.

### 4.2.3 Determination of shock response spectra for selected deterministic inputs

For a Dirac-delta shock input, and with Rayleigh or modal damping, the linearized system response has been shown to be a sum of easily determined, exponentially decaying sinusoids available in algebraic form (59). For rectangular-pulse and sawtooth inputs, the response would also include step and ramp components, and some time delays [6]. From these the remaining kinematic quantities behind common forms of shock response spectra could be found analytically as well, without requiring further convolution. See [5, 6, 7] for details.

## 4.3 Verification and Matlab Implementation

Two models were developed, and their respective shock responses compared, to verify the above equations. Both models describe an isotropic, homogeneous, aluminum test-plate: the first, an analytical model, implemented in Matlab; and the second, a linear finite-element (FEA) model, implemented in ANSYS. The plate material is 6061-T6 aluminum, with Young's modulus 69 GPa, mass density 2700 kg/m$^3$, Poisson's ratio 0.33, and modal damping ratio 0.02 (all modes). (See Fig. 3.) The plate is simply supported along each of its four edges, with dimensions 1.0 m x 0.75 m x 25 mm. Both models comprise uniform rectangular (parallelepiped) elements: 50 element divisions

along the length ($x$-direction, measured in the neutral plane from the lower left corner), and 38 along the width ($y$-direction, measured correspondingly). Impulses of identical strength (50 N-s) were applied at corresponding impact points, and the responses were determined at three sets of corresponding response points, from zero initial conditions.

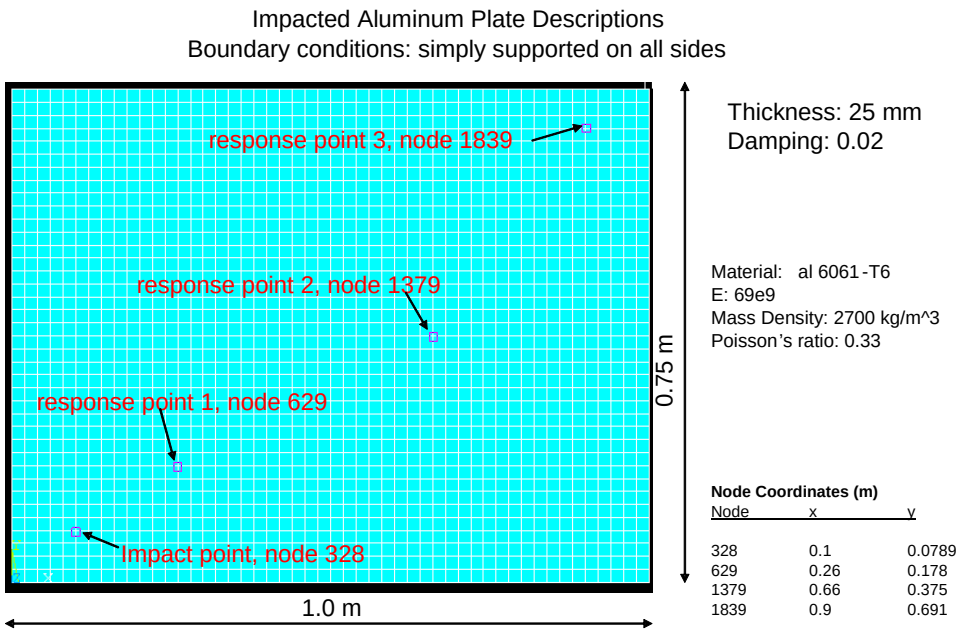


Figure 3. Test plate, showing impact- and response points

For the plots that follow the ($x$, $y$) coordinates of the impact and response points were (0.1, 0.0789) m and (0.66, 0.375) m, respectively. A single 10-µs symmetric sawtooth pulse (Fig. 4) was used for the finite-element model; the analytical model assumed an ideal (Dirac-delta) impulse. Twenty modes were used to determine the response of each model.

Figure 5 provides a side-by-side comparison of the 20 lowest modal frequencies (rad/s) from the respective models. In no case did the analytical frequency differ from the FEA frequency by more than 0.25 %. Figures 6 and 7 offer representative modeshape comparisons; and Figure 8 plots response-point displacements from the two models, at Node 1379 (refer to Fig. 3). The associated acceleration plots are shown in Figure 9. Corresponding modal frequencies, modeshapes, displacements, and accelerations all match well between the two models.

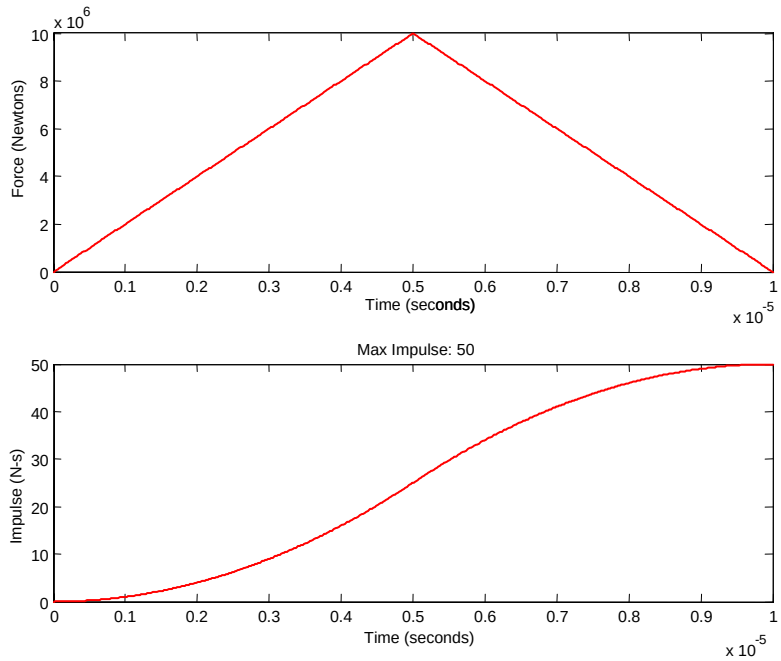


Figure 4. Loading function for FEA model

| FEA – Ansys | Analytical | Difference (%) |
|---|---|---|
| 168.6 | 168.6 | 0.015 |
| 350.6 | 350.7 | 0.030 |
| 492.2 | 492.4 | 0.027 |
| 654.0 | 654.3 | 0.041 |
| 674.1 | 674.5 | 0.061 |
| 977.1 | 978.0 | 0.093 |
| 1031.6 | 1032.0 | 0.042 |
| 1078.7 | 1079.3 | 0.052 |
| 1213.1 | 1214.2 | 0.085 |
| 1401.4 | 1403.0 | 0.119 |
| 1515.6 | 1517.7 | 0.137 |
| 1624.6 | 1625.6 | 0.065 |
| 1786.4 | 1787.5 | 0.061 |
| 1939.1 | 1942.7 | 0.185 |
| 1946.6 | 1949.4 | 0.142 |
| 1967.5 | 1969.6 | 0.108 |
| 2269.3 | 2273.2 | 0.173 |
| 2291.6 | 2293.4 | 0.079 |
| 2483.4 | 2489.0 | 0.228 |
| 2612.9 | 2617.2 | 0.163 |

Figure 5. Comparison of modal frequencies: 1st 20 modes

## Mode shape comparison

(6th mode, m = 3, n = 2)

FEA - ANSYS

Analytical - Matlab

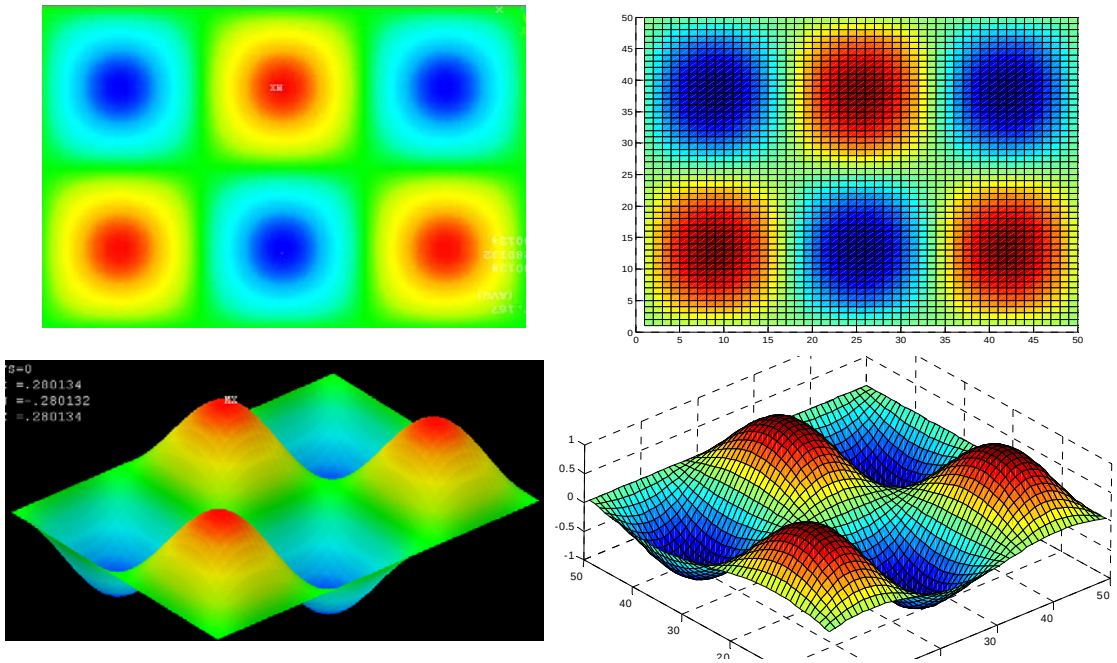


Figure 6. Modeshape comparison, 6th mode

## Mode shape comparison

(19th mode, m = 5, n = 3)

FEA - ANSYS

Analytical - Matlab

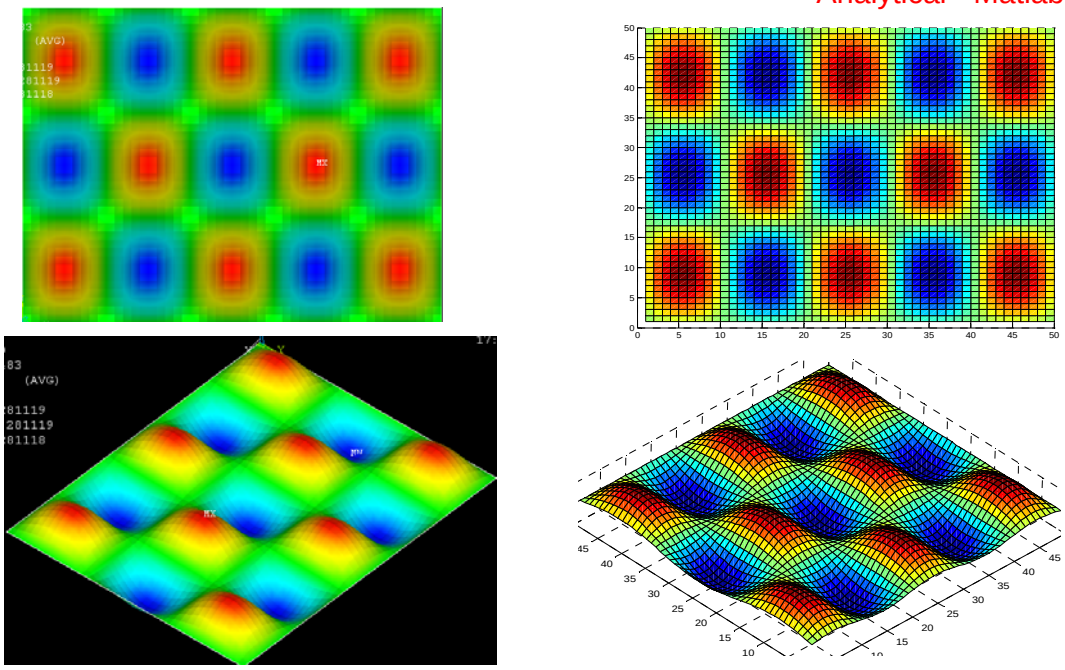


Figure 7. Modeshape comparison, 19th mode

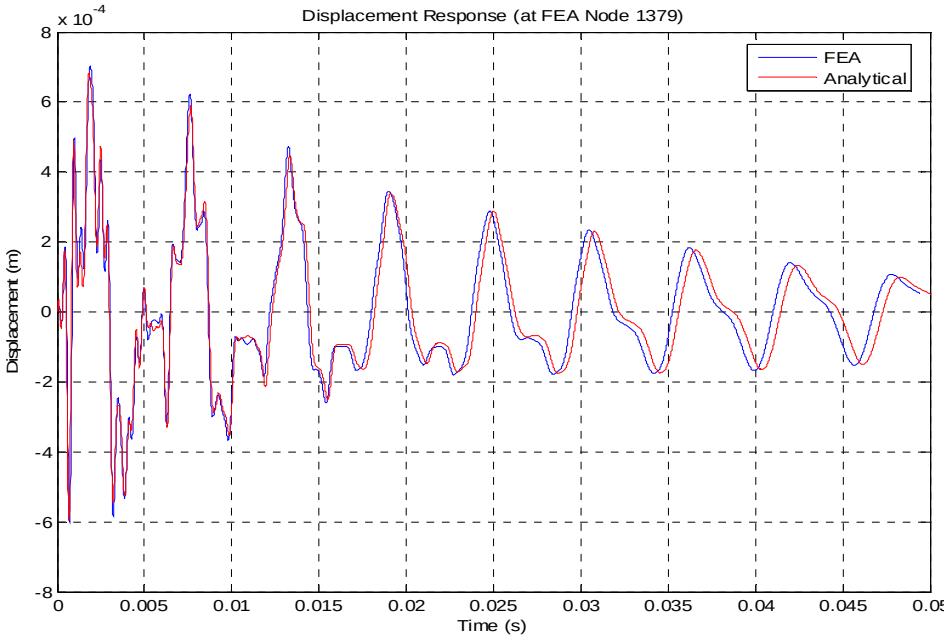


Figure 8. Response-point displacement comparison, node 1379, for an equal no. of elements (1900) and of modal components (20) in both models. Damping ratio: 0.02 for all modes.

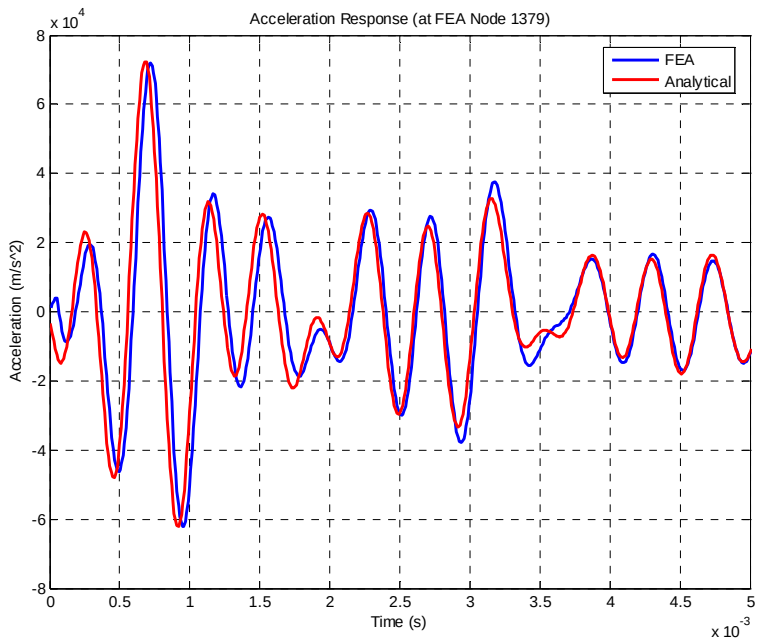


Figure 9. Response-point acceleration comparison, node 1379, for an equal no. of elements (1900) and of modal components (20) in both models. Damping ratio: 0.02 for all modes.

# 5 Case Two: Alternating Simple and Clamped Supports

## 5.1 Free Response of the Continuous Undamped Plate

Consider next the plate to be clamped on two opposing edges (those with dimension *a*, Fig. 2); simply supported on the other two edges (those with dimension *b*); and responding freely to nonzero initial conditions. The simply supported boundary conditions [9], as before, are represented by

$$w = w_{xx} + \nu w_{yy} = 0\,; \tag{60}$$

and the clamped conditions [9], by

$$w = w_y = 0\,. \tag{61}$$

As with the previous case, an analytical, modal solution to the homogeneous form of the differential equation is well known, for this plate geometry and set of boundary conditions (e.g., [8], pp. 45-50, and [9], pp. 259-264). Unfortunately, however, now the modal frequencies here cannot be found in explicit form; they must be found via the numerical solution of transcendental equations.

The solution has the form

$$w(x,y,t) = \sum_{m=1}^{\infty}\sum_{n=1}^{\infty} W_{mn}(x,y)\eta_{mn}(t) + \sum_{p=1}^{\infty}\sum_{q=1}^{\infty} \tilde{W}_{pq}(x,y)\tilde{\eta}_{pq}(t), \tag{62}$$

where $\eta_{mn}(t)$ and $\tilde{\eta}_{pq}(t)$ are modal coordinates corresponding, respectively, to modeshapes $W_{mn}(x,y)$ and $\tilde{W}_{pq}(x,y)$. The modal coordinates can be expressed as

$$\eta_{mn}(t) = \sin(\omega_{mn} t + \phi_{mn}) \tag{63}$$

and

$$\tilde{\eta}_{pq}(t) = \sin(\tilde{\omega}_{pq} t + \tilde{\phi}_{pq}), \tag{64}$$

for which modal frequency $\omega_{\mathrm{mn}}$ is the $n^{\mathrm{th}}$ lowest root of the following characteristic equation for a fixed value of *m*:

$$\sqrt{\omega^2 a^4 \frac{\rho}{D} - (m\pi)^4}\left[\cos\sqrt{\omega b^2\sqrt{\frac{\rho}{D}} - \left(\frac{m\pi b}{a}\right)^2}\,\cosh\sqrt{\omega b^2\sqrt{\frac{\rho}{D}} + \left(\frac{m\pi b}{a}\right)^2} - 1\right]$$
$$-(m\pi)^2 \sin\sqrt{\omega b^2\sqrt{\frac{\rho}{D}} - \left(\frac{m\pi b}{a}\right)^2}\,\sinh\sqrt{\omega b^2\sqrt{\frac{\rho}{D}} + \left(\frac{m\pi b}{a}\right)^2} = 0\,, \tag{65}$$

and modal frequency $\tilde{\omega}_{pq}$ is the $q^{\text{th}}$ lowest root of the characteristic equation:

$$\sqrt{\tilde{\omega}^2 a^4 \frac{\rho}{D} - (p\pi)^4} \left[ \cosh \sqrt{\tilde{\omega} b^2 \sqrt{\frac{\rho}{D}} - \left(\frac{p\pi b}{a}\right)^2} \cosh \sqrt{\tilde{\omega} b^2 \sqrt{\frac{\rho}{D}} + \left(\frac{p\pi b}{a}\right)^2} - 1 \right]$$
$$- (p\pi)^2 \sinh \sqrt{\tilde{\omega} b^2 \sqrt{\frac{\rho}{D}} - \left(\frac{p\pi b}{a}\right)^2} \sinh \sqrt{\tilde{\omega} b^2 \sqrt{\frac{\rho}{D}} + \left(\frac{p\pi b}{a}\right)^2} = 0 , \tag{66}$$

for a fixed value of $p$. Equation (65) serves as the characteristic equation for frequencies meeting the condition

$$\omega > \left(\frac{m\pi}{a}\right)^2 \sqrt{\frac{D}{\rho}} ; \tag{67}$$

and Equation (66), for frequencies satisfying

$$\tilde{\omega} < \left(\frac{p\pi}{a}\right)^2 \sqrt{\frac{D}{\rho}} . \tag{68}$$

To describe the associated modeshapes in compact form, first define the following, for convenience:

$$\mu_{mn} = \sqrt{\omega_{mn} \sqrt{\frac{\rho}{D}} - \left(\frac{m\pi}{a}\right)^2} , \tag{69}$$

$$\tilde{\mu}_{pq} = \sqrt{\tilde{\omega}_{pq} \sqrt{\frac{\rho}{D}} - \left(\frac{p\pi}{a}\right)^2} , \tag{70}$$

$$\nu_{mn} := \sqrt{\omega_{mn} \sqrt{\frac{\rho}{D}} + \left(\frac{m\pi}{a}\right)^2} , \tag{71}$$

and

$$\tilde{\nu}_{pq} := \sqrt{\tilde{\omega}_{pq} \sqrt{\frac{\rho}{D}} + \left(\frac{p\pi}{a}\right)^2} . \tag{72}$$

Then the modeshapes have the following descriptions:

$$W_{mn}(x, y) = C_{mn} \left[ (\cosh \nu_{mn} b - \cos \mu_{mn} b)(\mu_{mn} \sinh \nu_{mn} y - \nu_{mn} \sin \mu_{mn} y) \right.$$
$$\left. - (\mu_{mn} \sinh \nu_{mn} b - \nu_{mn} \sin \mu_{mn} b)(\cosh \nu_{mn} y - \cos \mu_{mn} y) \right] \sin \frac{m\pi x}{a} , \tag{73}$$

and $\tilde{W}_{pq}(x,y) = \tilde{C}_{pq}\left[\left(\cosh\tilde{\nu}_{pq}b - \cosh\tilde{\mu}_{pq}b\right)\left(\tilde{\mu}_{pq}\sinh\tilde{\nu}_{pq}y - \tilde{\nu}_{pq}\sinh\tilde{\mu}_{pq}y\right)\right.$

$$\left. - \left(\tilde{\mu}_{pq}\sinh\tilde{\nu}_{pq}b - \tilde{\nu}_{pq}\sinh\tilde{\mu}_{pq}b\right)\left(\cosh\tilde{\nu}_{pq}y - \cosh\tilde{\mu}_{pq}y\right)\right]\sin\frac{m\pi x}{a}. \qquad (74)$$

The coefficients $C_{mn}$ and $\tilde{C}_{pq}$, and the phase angles $\phi_{mn}$ and $\tilde{\phi}_{pq}$ are constants whose values depend on the initial conditions. Equations (63) through (74) complete the modal solution represented by Equation (62).

If the undamped natural frequencies (whether $\omega_{mn}$ or $\tilde{\omega}_{pq}$) are arranged in increasing order, then (removing the tildes, which are no longer needed) the double indices can be replaced with a single index *k*. Introduce also the symbols $\sin|\mathrm{h}$ and $\cos|\mathrm{h}$, each of which should be understood to represent either the indicated trigonometric or hyperbolic function, depending on the need. And use $\gamma_k$ to represent the value $\frac{m\pi}{a}$ or $\frac{p\pi}{a}$, as appropriate. The solution (62), then, becomes:

$$w(x,y,t) = \sum_{k=1}^{\infty} W_k(x,y)\eta_k(t); \qquad (75)$$

where the $k^{th}$ undamped natural frequency $\omega_k$ is a root of (65) or (66); the corresponding undamped modal coordinate is

$$\eta_k(t) = \sin(\omega_k t + \phi_k); \qquad (76)$$

and the associated modeshape $W_k(x,y)$ comes from (69), (71), and (73), or (70), (72), and (74), as appropriate:

$$W_k(x,y) = C_k\left[\left(\cosh\nu_k b - \cos|\mathrm{h}\,\mu_k b\right)\left(\mu_k\sinh\nu_k y - \nu_k\sin|\mathrm{h}\,\mu_k y\right)\right.$$

$$\left. - \left(\mu_k\sinh\nu_k b - \nu_k\sin|\mathrm{h}\,\mu_k b\right)\left(\cosh\nu_k y - \cos|\mathrm{h}\,\mu_k y\right)\right]\sin\gamma_k x. \qquad (77)$$

Define next the following constants, for convenience:

$$\beta_{1k} := \cosh\nu_k b - \cos|\mathrm{h}\,\mu_k b \qquad (78)$$

and

$$\beta_{2k} := \mu_k\sinh\nu_k b - \nu_k\sin|\mathrm{h}\,\mu_k b, \qquad (79)$$

Then (77) can be rewritten as

$$W_k(x,y) = C_k\left[\beta_{1k}\left(\mu_k\sinh\nu_k y - \nu_k\sin|\mathrm{h}\,\mu_k y\right)\right.$$

$$-\beta_{2k}\left(\cosh\nu_k y-\cos\text{h}\mu_k y\right)\Big]\sin\gamma_k x\,, \tag{80}$$

or, more compactly,

$$W_k(x,y)=C_k\,\psi_k(y)\sin\gamma_k\,x\,, \tag{81}$$

where $$\psi_k(y)=\beta_{1k}\left(\mu_k\sinh\nu_k y-\nu_k\sin\text{h}\,\mu_k y\right)-\beta_{2k}\left(\cosh\nu_k y-\cos\text{h}\mu_k y\right). \tag{82}$$

Equation (62) can now take the simple representative form,

$$w(x,y,t)=\sum_{k=1}^{\infty}\underbrace{\left[C_k\psi_k(y)\sin\gamma_k x\right]}_{W_k(x,y)}\eta_k(t)\,. \tag{83}$$

## 5.2 Forced Response of the Discretized Damped Plate

One can proceed as before with the simply-supported case. Application of the biharmonic operator to (83) leads directly to

$$\nabla^4 w=\nabla^4\left\{\sum_{k=1}^{\infty}\underbrace{\left[C_k\psi_k(y)\sin\gamma_k x\right]}_{W_k(x,y)}\eta_k(t)\right\}=\left\{\sum_{k=1}^{\infty}C_k\nabla^4\left[\psi_k(y)\sin\gamma_k x\right]\eta_k(t)\right\}. \tag{84}$$

Expanding $\nabla^4$ in terms of rectangular coordinates via (8), applying it to (84), and approximating the modal sum by the first $r$ terms, yields (after some effort)

$$\nabla^4 w=\frac{\rho}{D}\sum_{k=1}^{r}\omega_k^2 W_k(x,y)\eta_k(t)\,. \tag{85}$$

The modeshapes can be discretized into vector form:

$$\underline{u}_k=\begin{Bmatrix}W_k(x_1,y_1)\\ \vdots\\ W_k(x_r,y_r)\end{Bmatrix}=\begin{Bmatrix}C_k\,\psi_k(y_1)\sin\gamma_k\,x_1\\ \vdots\\ C_k\,\psi_k(y_r)\sin\gamma_k\,x_r\end{Bmatrix}, \tag{86}$$

which can again be normalized using the Euclidean norm (29). The remaining development of the shock-response equations is as presented before, from (30) through the end of Section 4. The general results are as given by (55), which, for the special case of zero initial conditions and single-point loading, simplifies to (58). If the loading is further idealized as a Dirac delta, (58) reduces again to (59). The shock response can then be used to determine the SRS at the response point of interest.

## 6 Conclusion

This paper has documented the development of a a constant- and lumped-parameter linear matrix model of a homogeneous, rectangular plate subject to transverse ballistic shock, for two classes of boundary conditions: (1) all edges in simple support, and (2) edges alternating between simple and clamped (fixed) support as one proceeds around the perimeter. Although the model was derived from a continuous (and exact) analytical model of an undamped plate, it was augmented to include either Rayleigh or modal damping. For each class the augmented equations were then solved analytically for the case of an ideal-impulse, transverse point-shock load. Matlab implementations ($1^{st}$ case only) were benchmarked against linear FEA models, with comparisons made using the first 20 modes. The frequencies, modeshapes, and displacement and acceleration responses all match well.

The model is provided in a form suitable for using a *one-time* eigen-analysis of a system to yield system kinematic responses that are useful, in turn, for various SRS determinations—that is, given an *arbitrary* impact-point/response-point pair. The enabled "same-plate" shock analysis, while not encompassing an entire military vehicle, would treat the most severe cases of shock response, for components mounted directly on the impacted plate.

## 7 Acknowledgments

The authors are grateful to the Army Research Laboratory (via the U.S. Military Academy's Mathematical Sciences Center of Excellence), and to the U.S. Military Academy's Department of Civil and Mechanical Engineering, for their funding of this work.

## 8 References

[1] Harris, Cyril M., and Piersol, Allan G., editors, *Harris' Shock and Vibration Handbook, Fifth Edition*, McGraw-Hill, NY, 2002, chap. 23, pp. 1-26.

[2] Gaberson, H. A., and Pal, D., "Shock Spectrum Classification of Violent Environments that Cause Machinery Failure," *Proceedings of the 18th International Modal Analysis Conference*, Feb. 2000, pp. 1126-1135.

[3] Smallwood, David O., "The Shock Response Spectrum at Low Frequencies," *Shock and Vibration Bulletin*, N. 56, Part 1, Aug. 1986, pp. 279-288.

[4] Gaberson, H. A., and Chalmers, Richard H., "Reasons for Representing Shock Spectra with Velocity as the Ordinate," *Proceedings of the 66th Shock and Vibration Symposium*, 1995, pp. 181-191.

[5] Hampton, R. David, Wiedenman, Nathan S., and Li, Ting H., "Analytical Determination of Shock Response Spectra, for an Impulse-Loaded Proportionally Damped System," ESDA 2004-58024, *Proceedings of the 7th Biennial Conference on Engineering Systems and Design Analysis*, July 2004. Also published with minor revision as "Quasi-Analytical Determination of Shock Response Spectra, for an Impulse-Loaded Proportionally Damped System," U-086, *Proceedings of the 75th Shock and Vibration Symposium*, October 2004.

[6] Hampton, R. David, Nygren, Kip P., and Li, Ting H., "Modal Expressions for Relative Displacements Underlying Pseudovelocity Shock-Response Spectra, for Idealized Remote Shock Loadings: Derivation and Verification," *Proceedings of the 76th Shock and Vibration Symposium*, October 2005.

[7] Hampton, R. David, Nygren, Kip P., Erickson, J., and Li, Ting H., "Analytical Kinematic Expressions for Pseudovelocity Shock Response Spectra of Generally Damped Linear Systems," *Proceedings of the 76th Shock and Vibration Symposium*, October 2005.

[8] Leissa, Arthur W., *Vibration of Plates*, NASA SP-160, 1969.

[9] Leissa, A. W., "The Free Vibration of Rectangular Plates," *Journal of Sound and Vibration*, Vol. 31, Part 3, 1973, pp. 257-293.

[10] Harris, Cyril M., and Piersol, Allan G., editors, *Harris' Shock and Vibration Handbook, Fifth Edition*, McGraw-Hill, NY, 2002, chap. 23, pp. 7.29-7.45.

[11] Hampton, R. David, Li, Ting H., and Nygren, Kip P., "Analytical Shock Response of a Transversely Point-Loaded Linear Rectangular Plate," *Proceedings of the 13th ARL/USMA Technical Symposium*, November 2005. Also published with minor changes as ESDA 2006-95608, *Proceedings of the 8th Biennial Conference on Engineering Systems and Design Analysis*, July 2006.